Damping and mechanical behavior of graphene nanoplatelets reinforced Al-30Zn alloy matrix bioinspired laminated composites by two steps flake powder metallurgy

Zheng Zhong[a,b] , Xiaosong Jiang[a,b*] , Hongliang Sun[a,b] , Peinan Du[c] *, Zixuan Wu[d] , Liu Yang[e]

[a]Key Laboratory of Advanced Technologies of Materials, Ministry of Education, Chengdu 610031, China

[b]School of Materials Science and Engineering, Southwest Jiaotong University, Chengdu Sichuan 610031, China

[c]Science and Technology on Reactor Fuel and Materials Laboratory, Nuclear Power Institute of China, Chengdu 610213, China

[d]School of Engineering and Materials Science, Queen Mary University of London, London E1 4NS, United Kingdom

[e]Institute for Applied Materials (IAM-WK), Karlsruhe Institute of Technology (KIT), Karlsruhe 76131, Germany

*Corresponding author: xsjiang@swjtu.edu.cn (X.S. Jiang), Tel./Fax: +86-28-87634177; OR dupeinan@126.com (P. Du), Tel./Fax: +86-28-85903839.

Abstract: Damping and mechanical properties are often incompatible in metallic materials. In this paper, bio-inspired laminated graphene nanoplatelets (GNPs) reinforced Al-30Zn alloy matrix composites with an outstanding combination of damping-mechanical properties are prepared using a flake powder metallurgy (FPM) process. The increased grain/phase boundary owing to grain refinement improves the intrinsic damping properties of the composites, while the lamellar grains promote the oriented alignment and crack deflection of GNPs. The multilayered GNPs with large specific surface area experienced

repeated stretching and compression during cyclic bending deformation, leading to intense interfacial frictional slip, and GNPs' high intrinsic thermal conductivity also helped to dissipate heat quickly, which promoted mechanical energy dissipation. The improvement in mechanical properties is mainly attributed to grain refinement, the load transfer effect of GNPs and their interaction with dislocations. The Al-30Zn-0.5GNPs composites showed the best combination of damping properties and mechanical properties.

Keywords: composites; characterization; powder methods; damping.

1. Introduction

Aluminum alloy, as a lightweight metal material, has the advantages of good casting performance, high strength, wide range of application, low price, etc., so it is widely used in aerospace, rail transportation and defense and military fields [1]. As modern industries develop rapidly, vibration and noise problems are becoming increasingly serious, and the damping performance of aluminum alloys has also become more demanding in engineering materials. However, the damping performance of common commercial aluminum alloys such as 6061 and 7075 is low [2, 3], which limits their application in engineering fields with high damping requirements, such as vibration damping washers, aerospace damping dampers, etc. [4]. While some zinc-aluminum alloys such as Zn-22Al have better damping capability, their high density (~6.16 g/cm^3) limits their applications [5]. How to achieve a balance between high damping and high mechanical strength is the key to achieve wider engineering applications of aluminum alloy materials. Therefore, the study of further improving the damping performance of aluminum alloys has high practical application value and important significance. Among the many grades of aluminum alloys, high-zinc aluminum alloys with 20-45 wt.% Zn additions [2, 6-10] have gained increasing attention for their excellent damping properties, which is attributed to the good wettability of

Al/Zn interface [11, 12]. The formation of fine Zn phases at grain boundaries and/or within Al grains through these special wetting interfaces improves the phase boundary sliding ability. However, the strength of Al-Zn alloys is lower than conventional commercial aluminum alloys [2, 7, 8]. Therefore, the damping-strength trade-off of Al-Zn alloys needs to be avoided as much as possible.

Damping capacity refers to a material's capacity to dissipate mechanical energy and convert it to other energy (such as heat), thereby reducing vibration and noise [13]. In vibration and noise reduction technology, the most economical and convenient way is to directly enhance the intrinsic damping performance of the material, and apply the high damping material directly to the vibration or noise source to prevent the vibration from propagating, rapidly reduce the amplitude of vibration and avoid resonance [14, 15]. However, for metallic materials, damping capacity is usually inversely dependent on stiffness and strength [16], because the microscopic mechanisms of strengthening and damping often overlap. Tight atomic bonds and high lattice friction contribute to the strength and toughness while tending to reduce the vibrational amplitude over time, resulting in low energy dissipation. Therefore, only when the mutual interference between the microscopic mechanisms of damping and strengthening is minimized can the optimal balance of desirable mechanical properties and damping capacity be realized [13, 14].

This ideal combination of properties can be attempted by developing multiphase composites, where each phase carries out a specific primary function: vibration damping or improvement of mechanical strength. Recently, there demand for lightweight structural materials such as AMCs with high damping capacity is increasing [17]. Compared with other high damping alloys, AMCs have the advantages of lightweight, high physical properties, simple process, low material cost, and good damping properties, etc. The use of Al matrix high damping materials is especially important for the aerospace, marine, and automobile manufacturing industries, which require lightweight structures with low vibration and noise

[17, 18]. Aluminum matrix composites (AMCs) with greater damping performance can be prepared by incorporating materials with good damping performance into Al matrix through the selection of reinforcements with different damping values, varying the content or distribution of reinforcement [19-23]. The damping mechanism of metal matrix composites (MMCs) can be classified into dislocation damping, interfacial damping, interaction damping, and hybrid damping rules [14, 24, 25]. The intrinsic energy dissipation mechanisms that GNPs possess, such as bending, flexing, sliding, and shearing of GNPs layers, make them promising for simultaneously enhancing mechanical and vibration damping performance of materials [26-28]. Lu [26] found that the damping value of the composites was twice as high as that of pure Al by performing uniaxial compression on reduced graphene oxide (RGO)/Al nanolaminate composite microcolumns, because more dislocations pile up at the RGO/Al interface. Based on Granato-Lücke dislocation theory [29], dislocation in polycrystalline metallic materials will act as a source of damping to promote elastic energy dissipation. Therefore, it′s possible that the RGO addition at the interlayer boundary enhances the dislocation clustering at the laminated Al grain boundary (GBs), especially near the boundary.

In this study, GNPs-reinforced Al-Zn alloy matrix composites with a pronounced lamellar structure were prepared by FPM and tested for damping properties and mechanical properties. In this research, the effects of lamellar structure and GNPs on damping and mechanical behavior of Al-30Zn-GNPs composites are investigated.

2. Experimental methods

2.1 Raw materials and preparation of composites

Commercial spherical Al powder (mean size: 20 μm, purity >99.9%), commercial spherical Zn

powder (mean size: 10 μm, >99.9%), and GNPs (<10 layers, purity >99%) were selected as raw materials. The Zn content in this experiment was kept at 30 wt.% and the selection of the matrix alloy composition was determined on the basis of extensive literature and research status studies [2, 6-10]. If the Zn content is too low, it will not be able to provide enough Zn/Al interfaces to dissipate energy; if the content of Zn is too high, the density of the prepared composites will also increase, which will not be able to satisfy the demand for the lightweighting of AMCs. The contents of the GNPs were selected to be 0 wt.%, 0.25 wt.%, 0.5 wt.%, and 1 wt.%. To investigate the influence of laminar structure on the damping and mechanical behavior of the composites, we also prepared non-lamellar Al-30Zn binary alloys using pristine spherical Al and Zn powders. After several explorations and comparisons, the ball milling times for Al and Zn powders were determined to be 180 min and 240 min, respectively. Other specific parameters of FPM and its post-treatment process can be found in our previous studies [30]. The composite powder was extruded at 30 MPa and vacuum sintered at a temperature of 480°C for 60 min. The preparation process of Al-30Zn-GNPs composites is shown in Fig. 1.

2.2 Characterization and Testing

The density of the specimens was measured by the drainage method according to Archimedes' principle. The phase of Al-30Zn-GNPs composites was confirmed by X-ray diffraction (XRD, X′Pert PRO). The microstructural analysis was carried out using scanning electron microscopy (SEM) (ZEISS Sigma 300) and transmission electron microscopy (TEM) (Talos F200X). The specimens used for the damping tests were 30 mm × 10 mm × 1 mm in size and were all machined parallel to the lamination direction, and the damping tests were conducted in single cantilever mode on a dynamic mechanical analysis (DMA) (Q800, TA). To evaluate the effect of strain amplitude (ε) variation on damping

performance, the vibration frequency (f) was kept at 1 Hz and ε ranged from 1.0×10^{-3}-1.0×10^{-1}. To evaluate the effect of f on the damping behavior of the material, ε was kept at 1.0×10^{-2}, and f ranged from 1-10 Hz. Mechanical tests were performed with a minimum of four specimens for each composite group at room temperature using a testing machine (WDW-3100) at a loading rate of 0.5 mm/min.

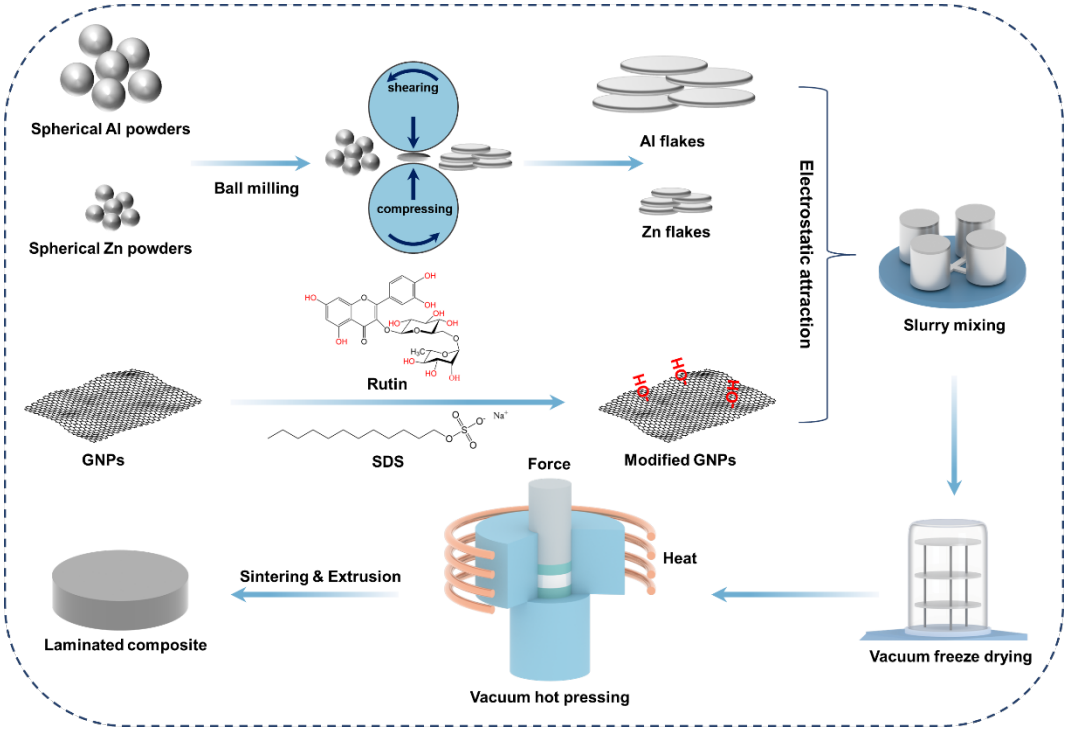

Fig. 1. Experimental flow chart.

3. Results and discussion

3.1 Powders

Fig. 2(a-b) show the pristine spherical Al and Zn powders, respectively, both of which have a uniform size distribution. Fig. 2(c) shows the composite powder made by mixing the ball-milled Al and Zn flakes, which obviously has a flatter 2D surface morphology and larger surface area compared with the pristine spherical powder before ball milling. The morphology and size of the matrix metal powder and the reinforcement are important factors in the formation of the laminar structure [31]. Spherical

pristine powders are continuously subjected to forward and lateral impacts from stainless steel balls during ball milling (Fig. 1), which deforms them into lamellar powders with flat surfaces. Such geometrical features can effectively improve their geometrical compatibility with GNPs, thus promoting the formation of lamellar structures and compositional homogenization in composites [31, 32]. The increase in surface energy during deformation of spherical Al and Zn powders adversely affects the uniform dispersion of GNPs, which leads to agglomeration of the metal powders [33].

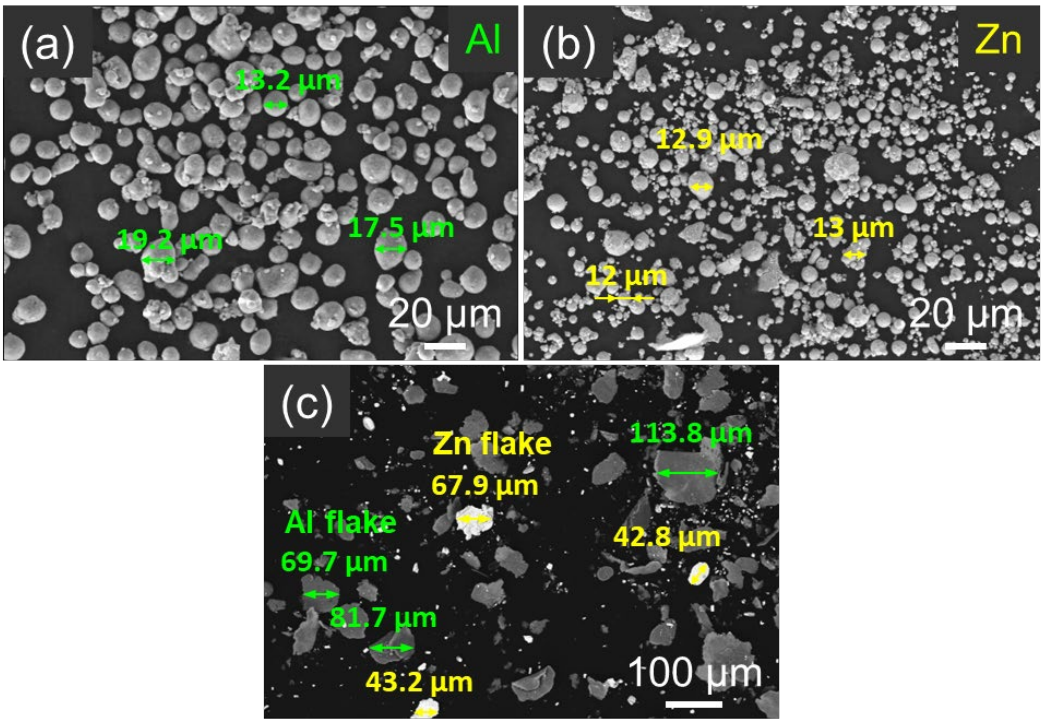

Fig. 2. SEM images of (a, b) original spherical Al powders and Zn powders, (c) Al and Zn flakes after ball-milling.

3.2 Microstructure analysis

Fig. 3 shows the microstructures of Al-30Zn(s) alloy as well as GNPs reinforced Al-30Zn alloy matrix composites. The grains of Al-30Zn(s) alloy sintered with pristine spherical powder showed a clear equiaxial shape (Fig. 3(a)), with a mean size of about 17.5 µm (Fig. 4). Large number of dispersed fine

white particles were observed at the grain boundaries, and the energy spectroscopy results indicated that these white particles are η-Zn precipitates, however, it can be observed that a clear segregation of η-Zn phase occurs at triple junctions of the grain boundaries (Fig. 3(b)). In metallic materials, such as alloys, segregation is a general phenomenon. Dissolved atoms are inclined to separate at grain boundaries to decrease the free energy of the system [34]. The reinforcement/matrix interface is a type of face defect and is likewise an ideal location for elemental segregation. Numerous studies have shown that element segregation at grain and phase boundary will influence interfacial properties such as bond strength, interfacial sliding, etc. [35, 36], which will be discussed in next part of this manual. The microstructure of Al-30Zn alloy sintered using flake powder is showed in Fig. 3(c-d), the grains exhibit a lamellar morphology which is significantly different from that in Fig. 3(a, b), with a mean size of about 5.8 μm, which is a 67% smaller than that of Al-30Zn(s) (Fig. 4). During the ball milling process, the impact of the stainless-steel balls on the metal powder leads to deformations such as flattening, cold welding and crushing, resulting in a reduction in the particle size of the base metal powder. Large plastic deformations lead to work hardening of the metal powder, which is then recrystallized during subsequent sintering to refine the grain size. A higher proportion of interfaces (grain or phase boundary) will promote internal friction during vibrations [24]. The η-Zn phase (mean size: 500 nm) precipitates finely and uniformly at the grain boundaries, and no significant segregation is observed. Fig. 3(e-h) shows the microstructures of Al-30Zn-GNPs, with the average grain sizes and morphologies essentially the same as those of Al-30Zn alloys. The high aspect ratio of the lamellae favors the formation of laminar structure after unidirectional pressing, and the GNPs are sandwiched between the layers of lamellar grains and wavy distributed parallel to the lamination direction, which is attributed to the confinement of the Al layer to the Zn and GNPs layers during extrusion, which makes them inclined to be aligned along the lamination

direction [37]. The weak van der Waals forces existing between the layers of GNPs allow them to exhibit a spring-like effect when subjected to applied compressive stresses in the direction of the outer layers, thus dissipating mechanical energy. The same holds true when graphene is bent or twisted at certain frequencies [28]. The interlayer sliding properties of multilayer GNPs will also consume additional energy as shear is transferred from Al grains to GNPs due to the load transfer function of GNPs [38]. The XRD patterns of Al-30Zn-GNPs composites are shown in Fig. 5, and the appearance of new corresponding characteristic peaks was not observed, indicating that the interfacial reaction did not take place or the reaction was extremely slight to the extent that it could not be observed by XRD.

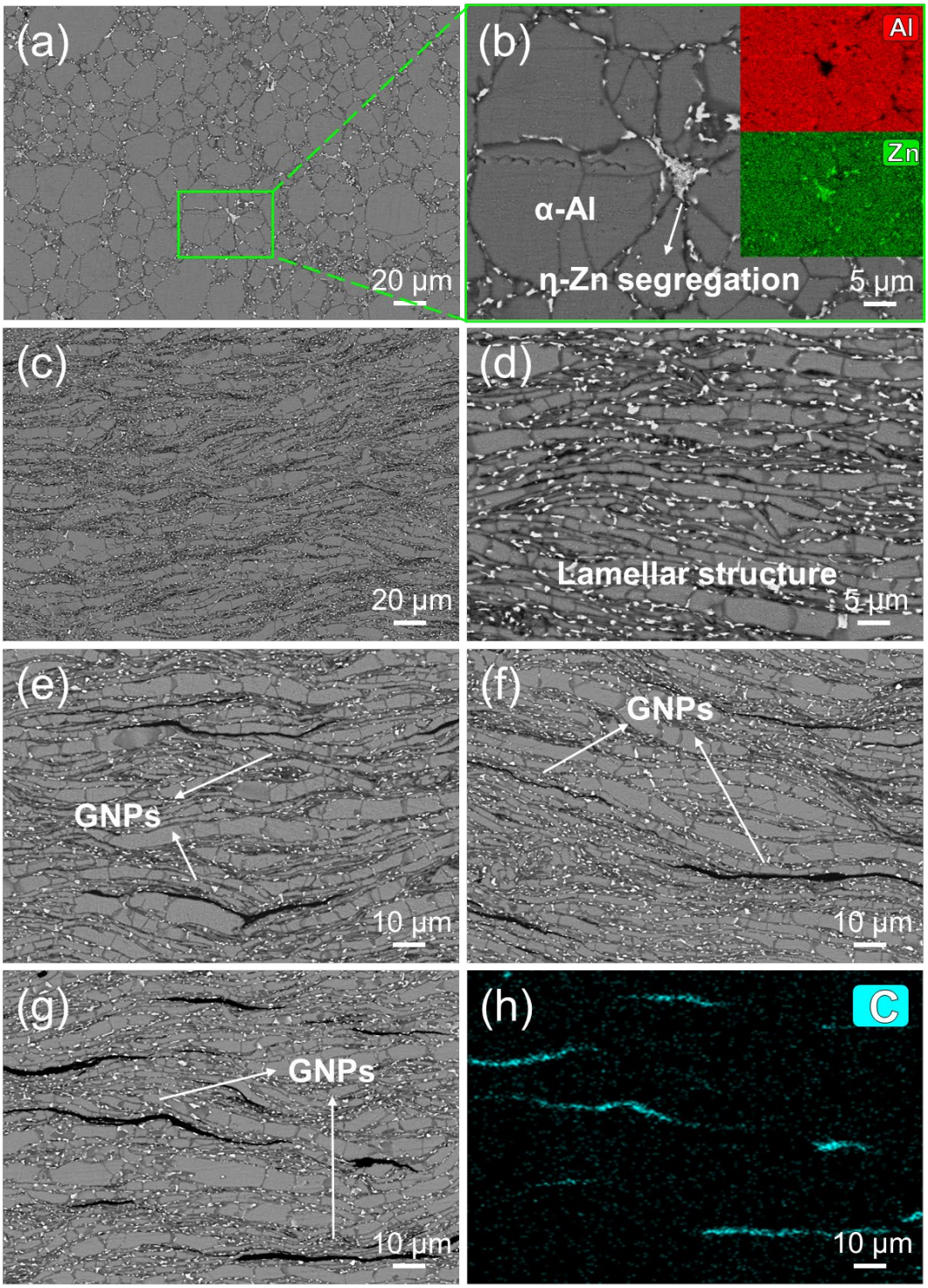

Fig. 3. SEM images of (a-b) Al-30Zn(s); (c-d) Al-30Zn; (e) Al-30Zn-0.25GNPs; (f) Al-30Zn-0.5GNPs; (g) Al-30Zn-1GNPs under BSE mode; (h) C distribution in (g).

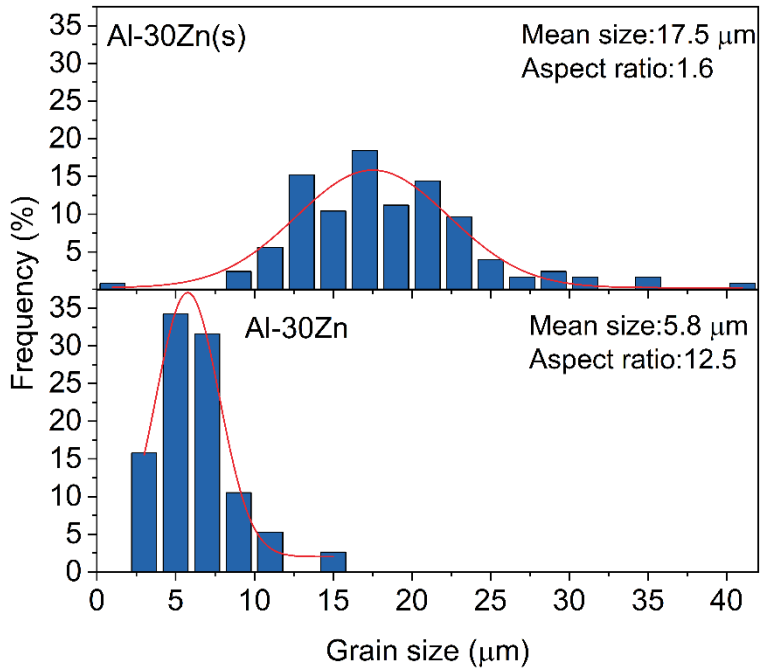

Fig. 4. Comparison of grain distribution between Al-30Zn(s) and Al-30Zn.

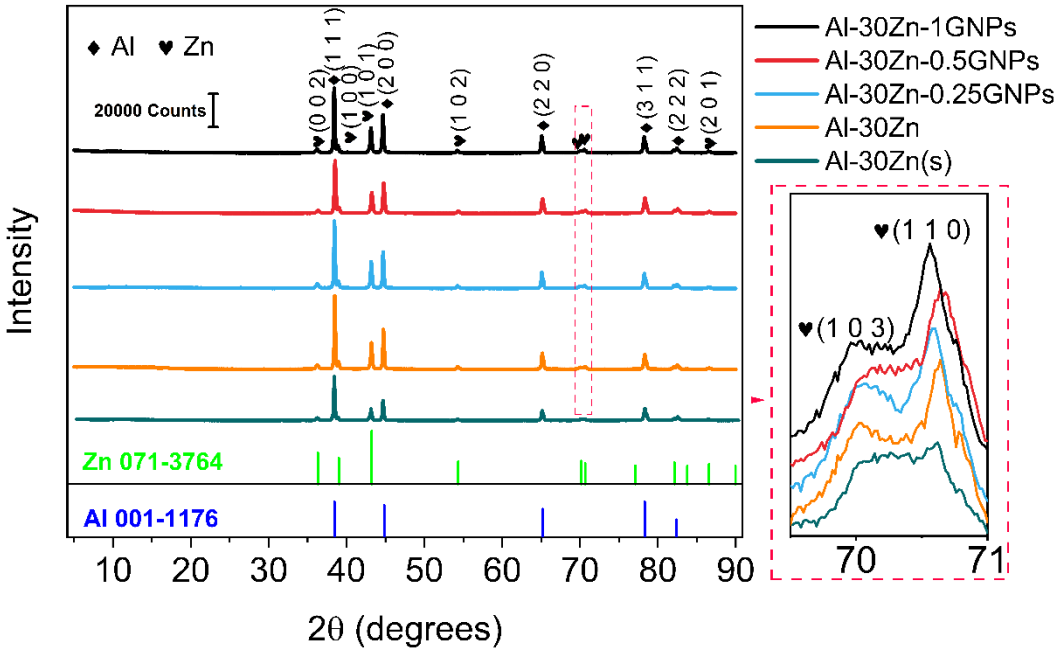

Fig. 5. XRD patterns of Al-30Zn-GNPs composites.

Fig. 6(a) shows the (high-angle annular dark-field) HAADF images and the related energy-dispersive X-ray spectroscopy (EDS) maps of micron-scale laminar structure of Al-30Zn-0.5GNPs composites, where the flat Al grains are obviously distributed parallel to the layers, and the GNPs with a large specific surface area are distributed between the neighboring Al grains as a "lubricant". From the

EDS map of Zn, it is obvious that there are two sizes of η-Zn precipitated phases in the composites with their own distribution characteristics, among which the sub-micron η-Zn (mean size: 1 μm) is mainly distributed around the grain boundaries and the GNPs, which is due to the high energy at grain boundaries promotes the coarsening of the precipitated Zn phases [7]; the nanoscale η-Zn (mean size: 50 nm), on the other hand, is all diffusely and uniformly distributed inside Al grains (Fig. 6(b)). These fine nanoscale precipitates are capable of pinning the dislocations and thus playing the effect of precipitate strengthening. Fig. 6(c-g) shows more details of the nanoscale precipitates in the composites. We found that the distribution of the intragranular nanoscale precipitates exhibits a clear directionality. High resolution TEM (HRTEM) images of η-Zn distributed along the Al $(1\ 1\ \bar{1})$ and Al $(1\ \bar{1}\ \bar{1})$ crystal planes are shown in Fig. 6(c) and (f), respectively, and fast Fourier transformation (FFT) images of the corresponding regions in Fig. 6(c) are shown in Fig. 6(d, e), respectively. The presence of dislocations is observed around the precipitates on the $(1\ 1\ \bar{1})$ crystal plane (indicated by bright green markers), as this is a common slip plane for dislocations in Al lattice [39]. Therefore, we could conclude that the habitual plane of the lamellar precipitates is the $\{1\ 1\ 1\}$ plane and is influenced by dislocation motion on these planes.

Fig. 6(g) is a localized enlarged view of the green box region in Fig. 6(c), and it is clear from the inverse FFT (IFFT) map of the corresponding phase that the Al/Zn interface exhibits a high coherency. For different interface types, the dislocation transport mechanism through the interface varies. Because the intersection of mismatched dislocations can be used as a preferential site to form an interfacial dislocation ring, interfaces with higher mismatches exhibit lower shear resistance than interfaces with lower mismatches. Due to the intrinsic discontinuity of dislocation slip across a semi-coherent interface, after the incoming dislocations have been absorbed and expanded their cores within the interface, in

order for them to be transferred to another crystal, slip transport will involve dislocation re-nucleation and exit into the efferent slip system process, which is often difficult to occur because of the thermal activation required for this process [40]. The dislocation core extension width increases with decreasing interfacial shear strength, and a weak shear interface with high mismatch will greatly hinder dislocation transport across the interface. Ma et al. [35] improved the coherency and bonding energy of Al/TiB_2 interface via conversion of the low-coherency TiB_2/Al interface to a high-coherency Al/Mg(Zn1.5Cu0.5)/TiB_2 multiphase interface, the formation of a large number of Orowan loops not only relieves the internal stresses, but also decomposes into prismatic loops, which provide new space for dislocation proliferation and annihilation [40], which increases the work-hardening rate and delays the onset of plastic instability by limiting the dislocation accumulation around the interface, thus achieving higher plasticity.

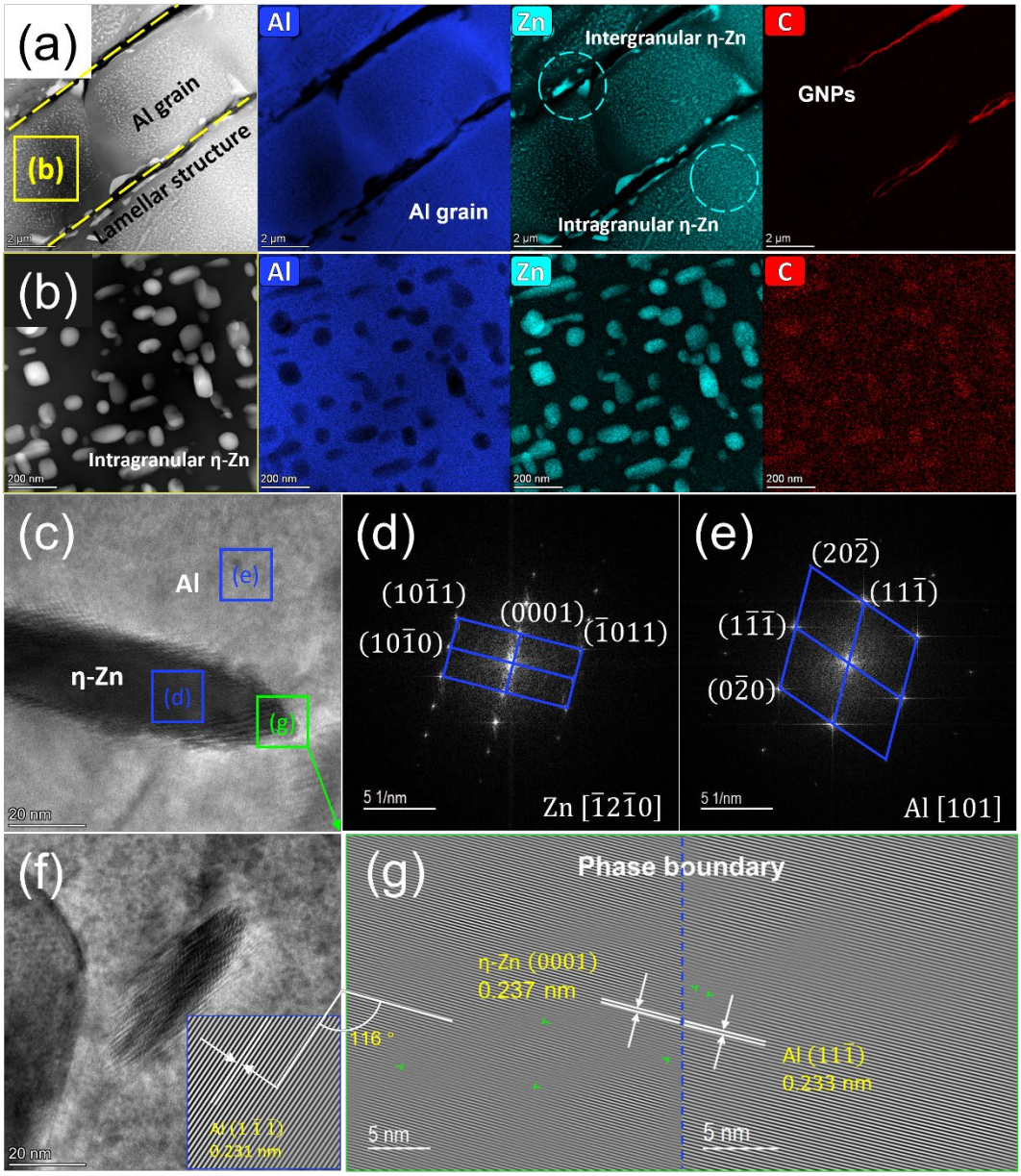

Fig. 6. (a) TEM-HAADF image of Al-30Zn-0.5GNPs composite and corresponding Al, Zn and C elemental EDS maps; (b) TEM-HAADF image showing homogeneous precipitates within Al grains and corresponding Al, Zn and C elemental EDS maps; (c) HRTEM image of η-Zn distributed along the $(11\bar{1})$ crystal plane; (d) and (e) FFT pattern of zone (d) and zone (e) in (c), respectively; (f) HRTEM image of η-Zn distributed along the $(1\bar{1}\bar{1})$ crystal plane; (g) IFFT pattern of zone (g) in (c), indicating high coherency of Zn/Al interface.

Fig. 7(a, b) shows the continuous and dense Al-30Zn/GNPs interfacial bonding, and the presence of

interfacial reaction products (e.g., Al_4C_3) is not observed, which is attributed to the more moderate sintering temperature (480 ℃). This is consistent with the study of Jiang [41], in which the formation of Al_4C_3 was not observed until above 540 ℃ in his study. The large aspect ratio of GNPs allows the GNPs/Al-30Zn interface to impede dislocation motion and store dislocations more effectively than Al grain boundaries, thus improving the work-hardening rate of the composites. Differences in physical properties (e.g., coefficient of thermal expansion (CTE) and elastic modulus (EM)) between the GNPs and the Al-30Zn alloy matrix induce geometrically necessary dislocations (GNDs) inside the grains when the material is cooled and processed, and the densities of these GNDs show a high-to-low distribution with the increase of the distance from the Al-30Zn/GNPs interface, and such a distribution pattern is intended to accommodate the strain gradient that arises when the material is deformed [41]. This process will promote the interaction between the interface and dislocations, and serves as GNDs strengthening. The tight GNPs/Al-30Zn alloy interfacial bonding can prevent the dislocation pile-up from leading to early crack initiation, and the composites will maintain good plasticity as a result. Fig. 7(c) shows the GNPs without significant structural damage, which helps to fully utilize its strengthening effects.

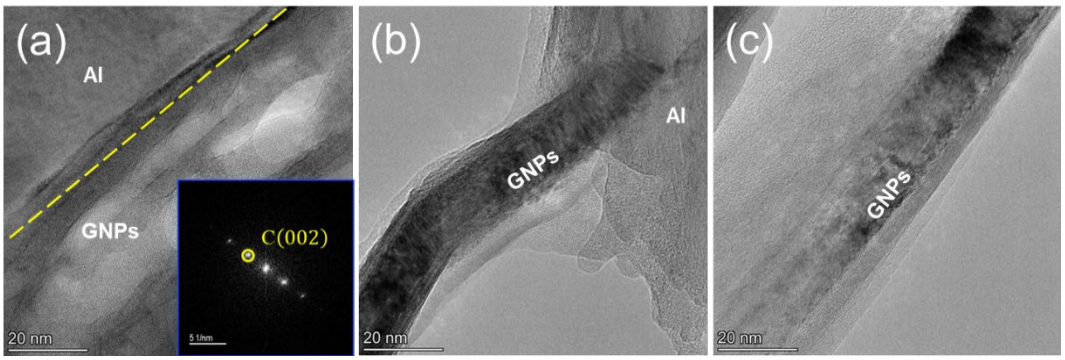

Fig. 7. Distribution and morphology of GNPs in the matrix. (a, b) Clean and tightly bonded Al/GNPs interface; (c) GNPs without structural damage.

3.3 Properties of the composites

3.3.1 Relative density

The relative densities of all specimens are shown in Fig. 8, and it is clear that the specimens sintered with flaky powder have higher relative densities (all above 95%) compared to those sintered with the original spherical powder. This is due to the higher aspect ratio of flaky metal powders and higher geometrical compatibility with the 2D morphology of the GNPs. During unidirectional pressing, the flake powders have a larger contact area with each other, which is favorable for atomic diffusion and sintering neck formation [31]. It is also observed that a very slight decrease in the densification of the specimens occurs as the content of GNPs increases, and the specimens maintain an extremely high densification (95.2%) even the content of GNPs has reached to 1 wt.%. The decrease in densification may be due to two reasons [42], one is the gap caused by the agglomeration of the reinforcement which makes it difficult for the sintered neck to fill it completely, and the other is the mismatch of CTE which may produce a certain amount of defects at the reinforcement/substrate interface.

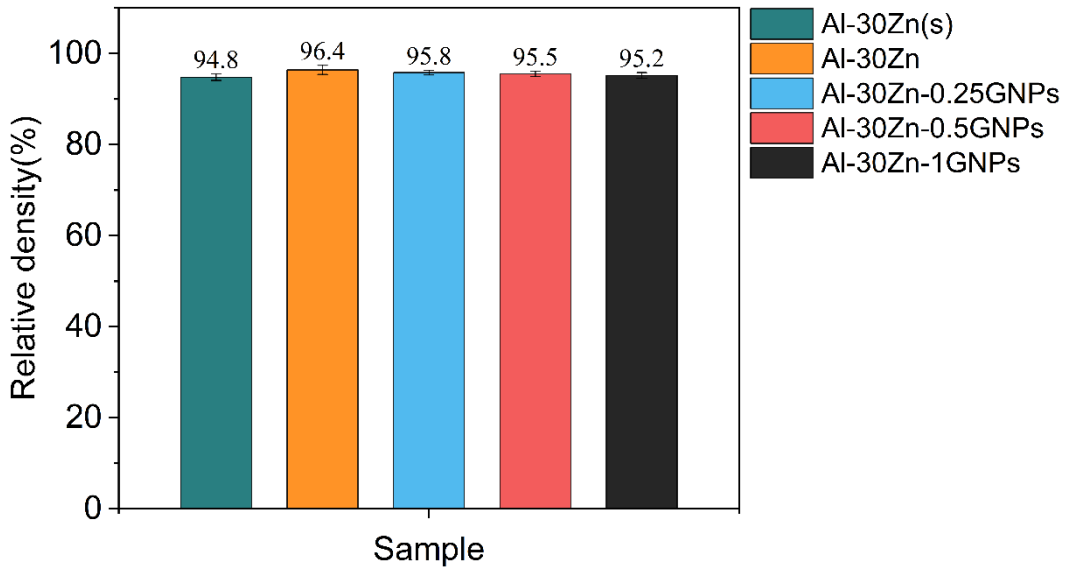

Fig. 8. Relative density of different samples.

3.3.2 Damping properties

Defect damping is the main damping mechanism for AMCs, since the damping is primarily attributed to the internal friction caused by cyclic motion of defects. Common sources of defect damping in composites include dislocations, grain boundaries and phase boundaries. Fig. 9 shows the loss tangent angle $\tan\delta$ and energy storage modulus E' variations of Al-Zn-GNPs composites at different frequencies and different strain amplitudes. The relationship between them can be expressed as follows:

$$\tan\delta = E''/E' \quad (1)$$

where E'' is the loss modulus. As shown in Fig. 9(a), the variation in the content of GNPs significantly affected the damping performance of Al-30Zn-GNPs composites, and their damping values were significantly higher than Al-30Zn alloy. Specifically, the damping performance of Al-30Zn alloy is slightly improved compared to Al-30Zn(s), which is attributed to the formation of lamellar grains and grain refinement increasing the grain boundary and phase boundary areas. Similar to dislocations, grain boundaries as a type of lattice defects can also affect damping performance of composites. Grain boundaries vibrate and internal friction increases when the strain amplitude exceeds a threshold value. Finer grain means more grain boundaries per unit volume, and more deformable grains means more energy is consumed by plastic flow between grains. Good interfacial lubricity typically correlates with high damping performance [43]. The Al/Zn phase boundary has good wettability, and these special wetting interfaces can enhance the interfacial sliding ability of Al-30Zn-GNPs composites [44, 45]. As showed in Fig. 3, lamellar grains promote more homogeneous Zn phase precipitation at GBs, whereas in Al-30Zn(s) alloys in observed a higher amount of Zn phase polarization at multiple junctions of Al grain boundaries. With the overall constant Zn content, the Zn segregation obviously reduces the overall area of Al/Zn interface in composites, which adversely affects the damping performance of Al-30Zn(s). During repeated bending and deforming, the wrinkled multilayer GNP with large specific surface area undergoes cyclic stretching and compression, resulting in intense interfacial frictional slip. Graphene's high intrinsic thermal conductivity helps dissipate thermal energy quickly, thus promoting mechanical energy dissipation [27]. At room temperature, the dislocation damping plays an important role in aluminum alloys and their composites, where the dislocation density, dislocation mobility and dislocation

length play significant role. According to Granato-Lücke dislocation theory [29], in metallic materials, high density dislocations will act as a damping source to promote elastic energy dissipation. Therefore, the addition of GNPs at the interlayer interfaces can promote the accumulation of dislocations at the interfaces of laminated Al grains, especially near the interfaces, and thus enhance the damping performance. It is worth noting that the slight increase in porosity with increasing GNPs content may also contribute to the increased damping performance, as vacancies or pores are able to dissipate energy through the defect damping mechanism [46, 47]. After introducing 0.25 wt.% of GNPs into Al-30Zn alloy, tan δ at the vibration frequency f=2 Hz increases from 9.1×10^{-3} to 1.28×10^{-2}, and the increase is up to 3.7×10^{-3}, and the increase decreases to 8.4×10^{-4} when the content of GNPs continues to be increased to 0.5 wt.%, and the increase is even reduced to 0% when GNPs content is further raised to 1 wt.%. The pattern can be found that as the content of GNPs increases, the damping performance enhancement decreases gradually. Clustering is inevitable with the addition of excess GNPs, and the subsequent reduction of reinforcement/matrix interface area may be the reason for the weakening of the enhanced damping effect of the high content of GNPs.

Furthermore, it's obvious that the change of vibration frequency f significantly affects the damping value of the material, regardless of whether GNPs are added or not, the $\tan\delta$ first falls rapidly and then rises slowly as the vibration frequency f increases (decreasing within 0.01-2Hz and increasing within 2-10Hz), and the change in the content of GNPs does not have any effect on the decrease or increase of the damping value, which indicates that this frequency-dependent change has nothing to do with GNPs, but is specific to the Al-Zn alloy itself. Changing the measurement frequency will only change the damping value, but not the nature of damping itself. When the temperature and strain amplitude are invariant and the vibration frequency is at a lower level, the source of dislocations is more likely to be activated, and as the vibration frequency decreases the density of moving dislocations gradually increases [48]. Therefore, based on the Granato-Lücke model [29], a higher damping capacity can be achieved at low frequency vibrations. However, as the vibration frequency f increases above 2 Hz, the damping value begins to increase slowly. As shown in Fig. 9(c), the storage modulus E' of all specimens remains

almost unchanged independent of the frequency change, so the damping value increment could only due to loss modulus E'' increment. The loss modulus is the amount of energy lost during viscous (irreversible) deformation of a material and reflects the magnitude of the material's viscosity. An increase in the loss modulus means an increase in energy dissipated by internal friction and grain deformation, because as the frequency of vibration increases, so does the frequency of interfacial friction. More mechanical energy is dissipated in a given period of time. Both vibration amplitude and frequency will affect the damping performance of Al-30Zn-GNPs composites because the larger the area swept by the dislocation the more energy is dissipated. However, as the frequency increases, the vibration amplitude of dislocations decreases [49, 50]. In conclusion, the nonlinear relationship between damping performance and vibration frequency is the result of the combined effect between reduced dislocation amplitude and increased vibration frequency.

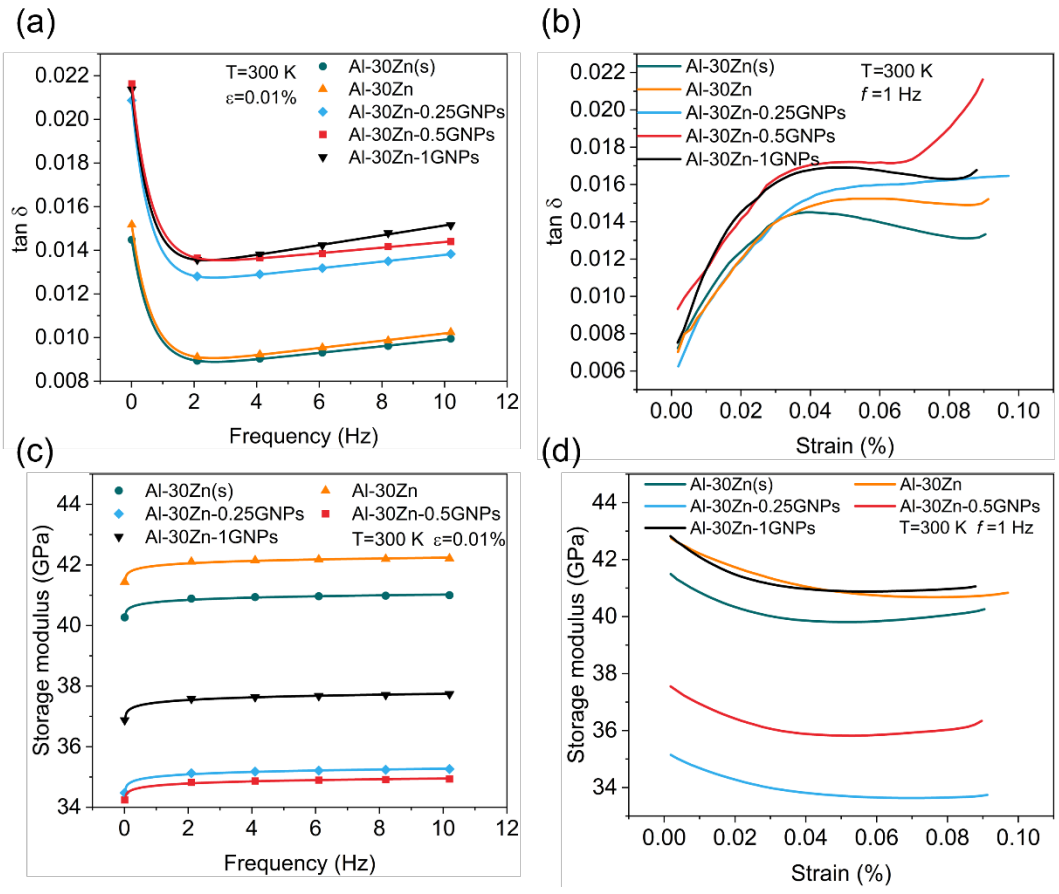

Fig. 9. (a) Frequency, (b) strain dependent damping capacity of Al-Zn-GNPs composites; (c) frequency, (d) strain dependent storage modulus of Al-Zn-GNPs composites.

Fig. 9(b) shows the damping performance of all specimen under different strain amplitudes (1Hz, 300K), and the variation of strain amplitude can significantly affect the damping performance. When the material is subjected to an external force, the neighboring grains move against each other, and the plastic rheology between the grains consumes energy, and at the same time, the viscous sliding under this plastic rheology is reversible, and the atoms return to their original position after the external stress is removed, and this process consumes energy, which brings about a significant damping effect. At constant vibration frequency and test temperature, the damping value increases with the increase of strain amplitude for all specimens. As the strain amplitude increases, the difference in $\tan\delta$ between Al-30Zn(s) alloy and Al-30Zn alloy gradually increases with increasing strain amplitude. This is due to the fact that Al-30Zn alloys have finer grains than those of Al-30Zn(s), and thus have more Al/Zn phase interfaces, and the advantage of interfacial damping at large strain amplitudes becomes more pronounced. The solid solubility of Zn in Al at room temperature is 2 wt.%, and the solute atoms are usually considered as weak pinning points that could efficiently peg dislocations at low amplitudes. As the strain amplitude rises, dislocations will escape from weak pinned points and be pinned by precipitated phase because of its stronger impeding ability on dislocations [48]. Therefore, with increasing strain amplitude, more dislocations are activated, leading to higher damping capacity. The addition of GNPs generally enhances the damping performance of composites; however, this does not mean the higher content of GNPs the better damping performance, which may be due to the agglomeration of the GNPs as well as their limitation of the grain motion. Overall, the Al-30Zn-0.5GNPs composites have the best damping properties, and the advantage becomes more obvious as the strain amplitude increases (after 0.07%). As

the strain amplitude increases, the stored energy modulus decreases for all specimens (Fig. 9(d)), which is favorable for the improvement of material damping properties.

Material	Processing technique	Damping capacity ($\tan\delta$)	ε (%)	Ref.
Al_p /7075Al	Hot rolling	0.0074	0.01	[3]
5086	Friction stir processing	0.004	0.01	[51]
7075	Friction stir processing	0.009	0.01	[51]
Al-20Zn (-0.5 Sc)	Hot rolling Solution treatment	<0.010	0.01	[7]
Al-35Zn	Friction stir processing	0.0073	0.05	[48]
	Solution treatment	0.0083		
	90% Hot rolling			
	50% Hot rolling + 80% Cold rolling	0.0137		
Al27.2Zn1.5Mg1.2Cu0.08Zr	Melt spinning+ hot extrusion	0.015	0.01	[52]
NiTi/AlSi10Mg	Selective laser melting	0.041	0.035	[53]
RHA(Rice husk ash)/A356.2	Stir casting	0.013	0.001	[54]
$NiTi_p$ /6061Al	FSP	0.003	0.01	[23]
Al-30Zn-0.5GNPs	FPM	0.015	0.01	This work

Table 1. Comparison of the $\tan\delta$ of Al-30Zn-0.5GNPs composites with other high damping Al alloys and AMCs at 1Hz and room temperature.

3.3.3 Tensile properties

The engineering stress-strain curves of all specimens are shown in Fig. 10. Comparing the tensile strengths of Al-30Zn(s) alloy and Al-30Zn alloy, it can be found that the strength (184.8 MPa) and

elongation (4.5%) of Al-30Zn with lamellar grain structure are significantly higher than that of Al-30Zn(s) (167.3 MPa, 3.2%). Since they have exactly the same composition, the enhancement in tensile strength is entirely attributable to their special laminated structure. The tensile strength of the composites increases and then decreases with the increasing mass fraction of GNPs, in which the Al-30Zn-0.5GNPs composite exhibits the best balance of strength and elongation (223.5 MPa, 5.1 %). In comparison with Al-30Zn(s) alloy, its strength and elongation increased by 34% and 59%, respectively. This is mainly attributed to the 2D planar structure of GNPs with large specific surface area for excellent load transfer, and the dislocation strengthening caused by GNPs hindering dislocation motion [55]. Considering that the material has not been heat-treated and thermally processed, the results obtained are satisfactory. However, by continuing to increase the content of GNPs, the mechanical properties of composites started to decrease simultaneously. When the concentration of GNPs exceeds the saturation level, agglomeration of GNPs will inevitably occur, and the strengthening efficiency of GNPs decreases drastically with the increase of GNPs content [37]. Excessive aggregation of GNPs at Al GBs is actually detrimental to the metallurgical bonding between the metal substrates, and with the gradual increase in applied stress these locations will become the starting point for crack initiation, leading to premature failure of the material.

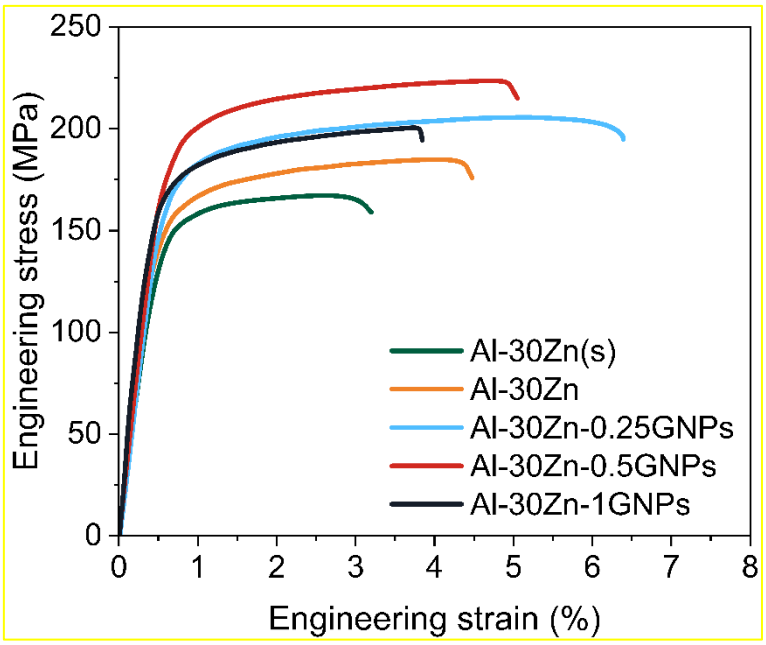

Fig. 10. Engineering stress-strain curve of all specimens with different GNPs contents.

3.4 Fractography

As shown in Fig. 11, the tensile fracture was observed with the help of SEM in secondary electron mode. A large number of coarse η-Zn precipitation phases as well as the presence of microcracks can be observed on the fracture of Al-30Zn(s) alloy, these microcracks apparently extend along the GBs. The incipient α-phase is an FCC structure with more slip systems and better plasticity, while the η-phase is an HCP structure with fewer slip systems and worse plasticity. As the interfacial shear stress increases and exceeds the Al/Zn interfacial bond strength, the interface debonds and microcracks begin to develop and expand. a clear "icing-sugar-like" fracture was observed on the fracture of the Al-30Zn(s) alloy (Fig. 11(a)). The discontinuous distribution of brittle precipitated phases on GBs (Fig. 11(b)) is the main reason for material failure. Comparing Figs. 11(a-b) and (c-f), it can be found that the construction of laminar structure has a considerable influence on the morphology of tensile fracture. The morphology of these fractures all exhibit distinct pearl layer characteristic, and numerous studies have found that this kind of

pearl-like laminar structure effectively promotes crack deflection and bridging [55]. Apart from this, the distribution of large-size Zn phases was not observed on the tensile fracture of specimens other than Al-30Zn(s) alloy. Undoubtedly this favors the mechanical properties of Al-30Zn-GNPs composites. As shown in Fig. 11(c-f), the fractured GNPs marked with red arrows uniformly distributed on the cross section indicate that fracture is the main failure behavior, which is due to the large aspect ratio of GNPs [56]. The modification of tensile fracture behavior of materials by GNPs through excellent load transfer effects and dislocation strengthening has been elucidated in a large number of related studies [26, 41, 56] and will not be discussed in detail here. It is possible to further improve the various properties of Al-30Zn-GNPs composites by improving the process conditions in order to optimize the precipitation behavior of Zn in the Al matrix, which will be carried out in our next work.

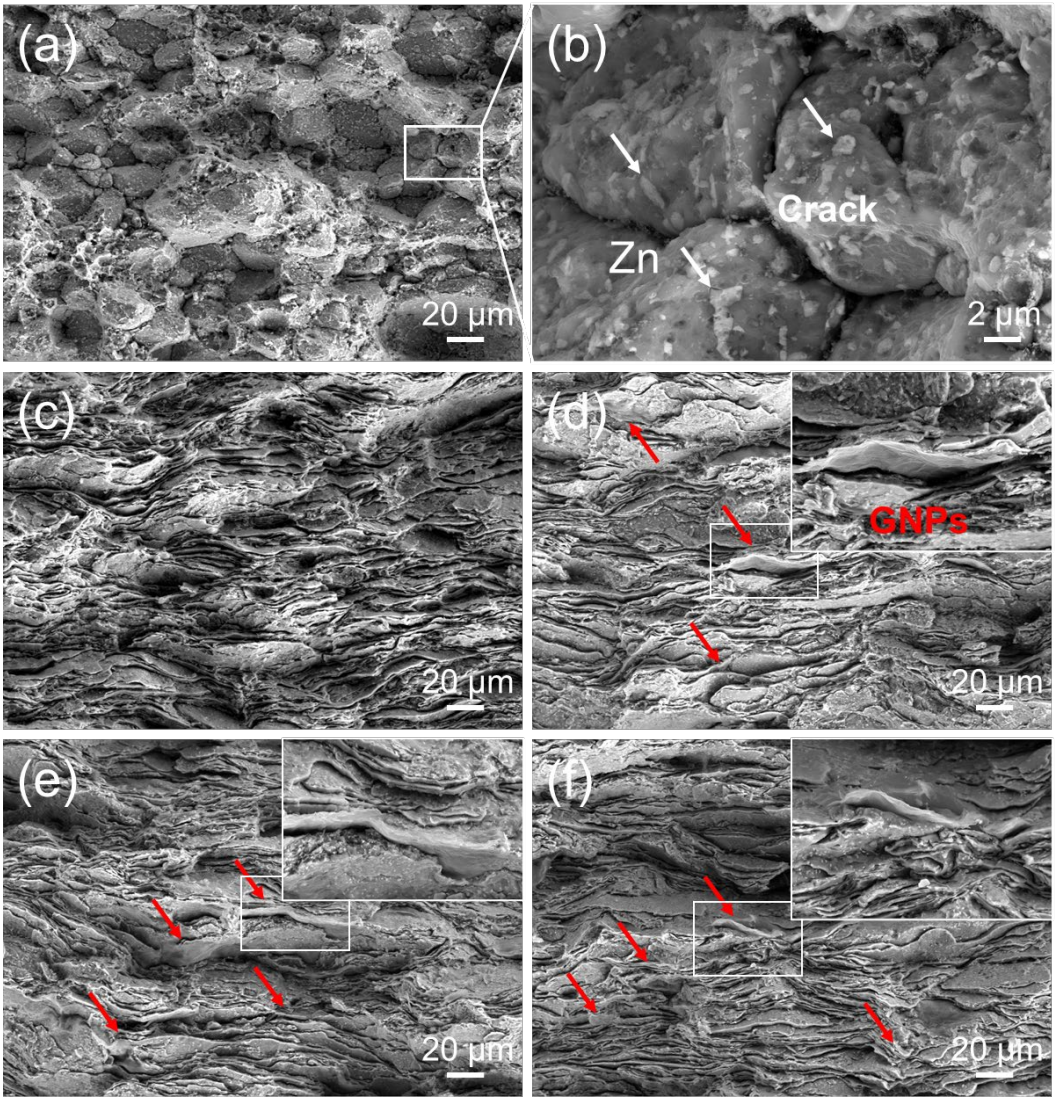

Fig. 11. Fracture surfaces of (a-b) Al-30Zn(s), (c) Al-30Zn, (d) Al-30Zn-0.25GNPs, (e) Al-30Zn-0.5GNPs, (f) Al-30Zn-1GNPs.

3.5. Discussion

The GNPs-reinforced Al-30Zn alloy matrix composites prepared in this study exhibit an excellent combination of damping and mechanical properties, and the main damping and strengthening mechanisms are shown in Fig. 12. Defect damping is the main damping mechanism, including interface damping and dislocation damping, and the improvement in damping performance is mainly ascribed to the intrinsic damping provided by grain refinement and the external damping provided by the

incorporation of moderate amounts of GNPs. The PBs between Al and Zn has good wettability, and these special wetting interfaces can improve the interfacial sliding ability of the Al- 30Zn alloy [44, 45]. The laminated composites prepared by the FPM process have finer lamellar grains, and the increase in the interfacial area is conducive to the enhancement of the intrinsic damping performance. During cyclic bending deformation, the GNPs with huge specific surface area experience repeated stretching and compression, leading to intense interfacial frictional slip, and the high thermal conductivity of GNPs facilitates rapid heat dissipation, which promotes mechanical energy dissipation [27].

The strength improvement of GNPs reinforced Al-30Zn alloy matrix composites may mainly come from three strengthening mechanisms: grain refinement due to FPM process, load transfer effect of GNPs, and dislocation strengthening due to the incorporation of GNPs. The fine grain strengthening was determined by using the Hall-Petch equation. According to this equation, the yield strength increases with decreasing grain size. The GBs can serve as effective obstacles to dislocation slip, and as the grain size decreases, the density in the grain boundary region increases, thereby increasing the strength. The increase in yield strength due to grain refinement can be calculated according to the following equation:

$$\sigma_{gb} = \sigma_0 + kd^{-1/2} \tag{2}$$

Where σ_0 =35 MPa (roughly equivalent to the yield strength of single crystal) [57]; k = 120 MPa (a constant characterizing the extent to which GBs affect strength, related to the structure of the GBs) [58]; d is the average diameter of the polycrystals. From the statistical data in Fig. 4, it can be obtained that the average grain size of Al-30Zn(s) alloy is about 17.5 μm and that of Al-30Zn alloy is about 5.8 μm, and the results obtained by substituting into the above equations are 63.7 MPa and 84.8 MPa, respectively, so the strength enhancement $\Delta\sigma_{gb}$ caused by the fine-grain strengthening is 21.1 MPa. Considering the presence of calculation and statistical errors, this value is close to the value obtained from the mechanical

properties test (16 MPa) and is therefore reliable.

GNPs improve the toughness of the Al-30Zn alloy matrix through load transfer effects, hindering dislocation motion to promote dislocation strengthening, and crack deflection and bridging, and the tight interfacial bonding with Al-30Zn matrix is the guarantee of the strengthening efficiency of GNPs [41]. The excellent intrinsic properties of graphene, high aspect ratio, and large interfacial contact area with the metal matrix allow for excellent load transfer efficiency in composites. The large surface area of GNPs and their effective hindrance to dislocation slip make the GNPs/Al-30Zn interface a favorable location for dislocation storage, which induces stronger dislocation strengthening effects. Differences in physical properties (e.g., CTE and EM) between the GNPs and the Al-30Zn alloy matrix induce GNDs inside the grains when the material is cooled and processed, and the densities of these GNDs show a high-to-low distribution with the increase of the distance from the Al-30Zn/GNPs interface, and such a distribution pattern is intended to accommodate the strain gradient that arises when the material is deformed [41]. The firm GNPs/Al-30Zn interfacial bonding can prevent the dislocation buildup from leading to early crack initiation, and the composites will maintain good plasticity as a result.

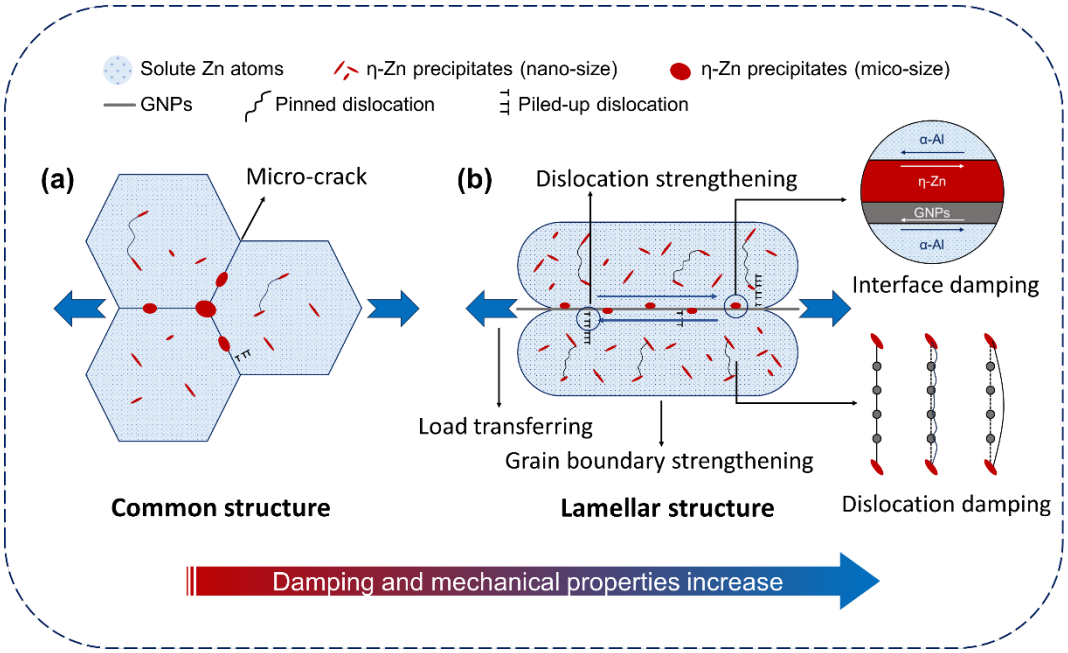

Fig. 12. Schematic illustration of the damping and strengthening mechanism by comparing (a) original Al-30Zn alloy and (b) in Al-30Zn-GNPs laminated composites.

4. Conclusions

In this paper, GNPs-reinforced Al-30Zn alloy matrix laminated composites were fabricated through FPM process, and the effects of laminated structure and GNPs incorporation on the damping and mechanical behavior of Al-30Zn-GNPs composites were systematically investigated. The conclusions can be summarized as follows:

1) Flake Al and Zn powders with high specific surface area were prepared by the FPM process, and their geometrical compatibility with GNPs was significantly improved. This greatly facilitated the homogenization of the matrix composition, the uniform and oriented distribution of GNPs, and the effect of fine laminated structures construction. The advantages of the pearl layer-inspired laminar structure in balancing the mechanical and damping properties lie in the refinement of grains, improvement of interfacial bonding, and increase of interfacial area.

2) For the GNPs reinforced Al-30Zn alloy matrix laminated composites, defect damping is the main damping mechanism, including interface damping and dislocation damping, and the improvement in damping performance is mainly ascribed to the intrinsic damping provided by grain refinement and the external damping provided by the incorporation of moderate amounts of GNPs. The laminated composites prepared by FPM have finer lamellar grains, and the increase in the interfacial area is conducive to the enhancement of the intrinsic damping performance of the composites. During cyclic bending deformation, the GNPs with huge specific surface area experienced repeated stretching and compression, leading to intense interfacial frictional slip, and the high intrinsic

thermal conductivity of graphene also contributes to the rapid heat dissipation, thus promoting the mechanical energy dissipation.

3) The construction of laminated structure can effectively promote crack deflection and retard crack extension to provide external toughening. GNPs improve the toughness of Al-30Zn alloys through load transfer, hindering dislocation motion, and crack bridging, and the tight interfacial bonding with the alloy matrix is the guarantee of the strengthening effect of GNPs.

Conflict of interest

The authors declare that they have no conflict of interest.

Acknowledgments

This work was supported by Key Laboratory of Infrared Imaging Materials and Detectors, Shanghai Institute of Technical Physics, Chinese Academy of Sciences (No. IIMDKFJJ-21-10) and China Postdoctoral Science Foundation (No. 2018T110993). We would like to thank Analytical and Testing Center of Southwest Jiaotong University for partial testing.

Data Availability statement

The data used to support the findings of this study are available from the corresponding author upon request.

References

[1] W. Li, S. Li, J. Liu, A. Zhang, Y. Zhou, Q. Wei, C. Yan, Y. Shi, Effect of heat treatment on AlSi10Mg alloy fabricated by selective laser melting: Microstructure evolution, mechanical properties and fracture mechanism, Mater. Sci. Eng. A-Struct. Mater. Prop. Microstruct. Process. 663 (2016) 116-125. https://doi.org/10.1016/j.msea.2016.03.088.

[2] C. Liu, B. Zhang, Z. Ma, H. Jiang, W. Zhou, Effect of Sc addition, friction stir processing, and T6 treatment on the damping and mechanical properties of 7055 Al alloy, J. Alloy. Compd. 772 (2019) 775-781. https://doi.org/10.1016/j.jallcom.2018.09.109.

[3] Y. Wang, H. Jiang, C. Liu, H. Huang, L. Wei, F. Qin, Influence of Al particle layer on damping behavior of Alp/7075Al composites fabricated by hot rolling, J. Alloy. Compd. 882 (2021) 160763. https://doi.org/10.1016/jjallcom.2021.160763.

[4] J.P. Immarigeon, R.T. Holt, A.K. Koul, L. Zhao, W. Wallace, J.C. Beddoes, Lightweight materials for aircraft applications, Mater. Charact. 35 (1995) 41-67. https://doi.org/10.1016/1044-5803(95)00066-6.

[5] Z. Zhang, F. Xiao, Y. Wang, Y. Jiang, Mechanism of improving strength and damping properties of powder-extruded Al/Zn composite after diffusion annealing, Trans. Nonferrous Met. Soc. China 28 (2018) 1928-1937. https://doi.org/10.1016/s1003-6326(18)64838-1.

[6] T. Savaskan, Y. Alemdag, Effect of nickel additions on the mechanical and sliding wear properties of Al-40Zn-3Cu alloy, Wear 268 (2010) 565-570. https://doi.org/10.1016/j.wear.2009.10.002.

[7] Y. Chen, C. Liu, Z. Ma, H. Huang, Y. Peng, Y. Hou, Effect of Sc addition on the microstructure, mechanical properties, and damping capacity of Al-20Zn alloy, Mater. Charact. 157 (2019) 109892. https://doi.org/10.1016/j.matchar.2019.109892.

[8] H. Jiang, C. Liu, Y. Chen, Z. Yang, H. Huang, L. Wei, Y. Li, H. Qi, Evaluation of microstructure,

damping capacity and mechanical properties of Al-35Zn and Al-35Zn-0.5Sc alloys, J. Alloy. Compd. 739 (2018) 114-121. https://doi.org/10.1016/j.jallcom.2017.12.234.

[9] W. Wang, D. Yi, W. Hua, B. Wang, High damping capacity of Al-40Zn alloys with fine grain and eutectoid structures via Yb alloying, J. Alloy. Compd. 870 (2021) 159485. https://doi.org/10.1016/j.jallcom.2021.159485.

[10] Y. Alemdag, T. Savaskan, Mechanical and tribological properties of Al-40Zn-Cu alloys, Tribol. Int. 42 (2009) 176-182. https://doi.org/10.1016/j.triboint.2008.04.008.

[11] R.Z. Valiev, M.Y. Murashkin, A. Kilmametov, B. Straumal, N.Q. Chinh, T.G. Langdon, Unusual super-ductility at room temperature in an ultrafine-grained aluminum alloy, J. Mater. Sci. 45 (2010) 4718-4724. https://doi.org/10.1007/s10853-010-4588-z.

[12] S. Shin, G. Yeom, T. Kwak, I. Park, Microstructure and mechanical properties of TiB-containing Al–Zn binary alloys, J. Mater. Sci. Technol. 32 (2016) 653-659. https://doi.org/10.1016/j.jmst.2016.04.016.

[13] A. Treviso, B. Van Genechten, D. Mundo, M. Tournour, Damping in composite materials: properties and models, Compos. Pt. B-Eng. 78 (2015) 144-152. https://doi.org/10.1016/j.compositesb.2015.03.081.

[14] H. Lu, X. Wang, T. Zhang, Z. Cheng, Q. Fang, Design, fabrication, and properties of high damping metal matrix composites-a review, Materials 2 (2009) 958-977. https://doi.org/10.3390/ma2030958.

[15] O.E. Ozbulut, S. Hurlebaus, R. Desroches, Seismic response control using shape memory alloys: a review, J. Intell. Mater. Syst. Struct. 22 (2011) 1531-1549. https://doi.org/10.1177/1045389x11411220.

[16] G. Li, Y. Ma, X. He, W. Li, P. Li, Damping capacity of high strength-damping aluminum alloys prepared by rapid solidification and powder metallurgy process, Trans. Nonferrous Met. Soc. China 22 (2012) 1112-1117. https://doi.org/10.1016/s1003-6326(11)61291-0.

[17] J. Shin, K. Choi, S. Shiko, H. Choi, D. Bae, Mechanical damping behavior of Al/C60-fullerene composites with supersaturated Al-C phases, Compos. Pt. B-Eng. 77 (2015) 194-198. https://doi.org/10.1016/j.compositesb.2015.03.006.

[18] E. Piollet, E.R. Fotsing, A. Ross, G. Michon, High damping and nonlinear vibration of sandwich beams with entangled cross-linked fibres as core material, Compos. Pt. B-Eng. 168 (2019) 353-366. https://doi.org/10.1016/j.compositesb.2019.03.029.

[19] C. Liu, L. Yu, Z. Ma, Y. Liu, C. Liu, H. Li, H. Wang, Damping capacity of Al–12Si composites effected by negative thermal expansion of Y2W3O12 particle inclusions, J. Mater. Res. Technol-JMRT 9 (2020) 9985-9995. https://doi.org/10.1016/j.jmrt.2020.07.008.

[20] M. Gui, D. Wang, J. Wu, G. Yuan, C. Li, Deformation and damping behaviors of foamed Al-Si-SiCp composite, Mater. Sci. Eng. A-Struct. Mater. Prop. Microstruct. Process. 286 (2000) 282-288. https://doi.org/10.1016/s0921-5093(00)00789-9.

[21] Y. Zhang, N. Ma, H. Wang, Y. Le, S. Li, Effect of Ti and Mg on the damping behavior of in situ aluminum composites, Mater. Lett. 59 (2005) 3775-3778. https://doi.org/10.1016/j.matlet.2005.06.055.

[22] Y. Gao, X. Wang, W. Jiang, J. Yang, L. Zeng, Q. Fang, High damping capacity and low density M2052/Al composites fabricated by accumulative roll bonding, J. Alloy. Compd. 757 (2018) 415-422. https://doi.org/10.1016/j.jallcom.2018.05.104.

[23] D. Ni, J. Wang, Z. Ma, Shape memory effect, thermal expansion and damping property of friction stir processed NiTip/Al composite, J. Mater. Sci. Technol. 32 (2016) 162-166. https://doi.org/10.1016/j.jmst.2015.12.013.

[24] E.J. Lavernia, R.J. Perez, J. Zhang, Damping behavior of discontinuously reinforced Al-alloy metal-matrix composites, Metall. Mater. Trans. A-Phys. Metall. Mater. Sci. 26 (1995) 2803-2818.

https://doi.org/10.1007/bf02669639.

[25] J. Zhang, R.J. Perez, C. Wong, E.J. Lavernia, Effects of secondary phases on the damping behavior of metals, alloys and metal matrix composites, Mater. Sci. Eng. R-Rep. 13 (1994) 325-389. https://doi.org/10.1016/0927-796x(94)90010-8.

[26] A. Lu, L. Zhao, Y. Liu, Z. Li, D. Xiong, J. Zou, Q. Guo, Enhanced damping capacity in graphene-Al nanolaminated composite pillars under compression cyclic loading, Metall. Mater. Trans. A-Phys. Metall. Mater. Sci. 51 (2020) 1463-1468. https://doi.org/10.1007/s11661-020-05632-4.

[27] H. Wang, C. Ma, W. Zhang, H. Cheng, Y. Zeng, Improved damping and high strength of graphene-coated nickel hybrid foams, ACS Appl. Mater. Interfaces 11 (2019) 42690-42696. https://doi.org/10.1021/acsami.9b10382.

[28] D. Lahiri, S. Das, W. Choi, A. Agarwal, Unfolding the damping behavior of multilayer graphene membrane in the low-frequency regime, ACS Nano 6 (2012) 3992-4000. https://doi.org/10.1021/nn3014257.

[29] A. Granato, K. Lücke, Theory of mechanical damping due to dislocations, J. Appl. Phys. 27 (1956) 583-593. https://doi.org/10.1063/1.1722436.

[30] Z. Zhong, X. Jiang, X. Wang, H. Sun, P. Du, Z. Wu, L. Yang, Enhanced strength and ductility in nanocarbon hybrid reinforced B4C/Al laminated composites fabricated by vacuum hot pressing, Vacuum 218 (2023) 112651. https://doi.org/10.1016/j.vacuum.2023.112651.

[31] X. Wang, X. Jiang, H. Sun, Y. Zhang, Y. Fang, R. Shu, Microstructure and mechanical properties of bioinspired laminated Al matrix hybrid reinforced with B4C and graphene nanoplatelets, Mater. Charact. 193 (2022) 112307. https://doi.org/10.1016/j.matchar.2022.112307.

[32] L. Jiang, Z. Li, G. Fan, L. Cao, D. Zhang, The use of flake powder metallurgy to produce carbon

nanotube (CNT)/aluminum composites with a homogenous CNT distribution, Carbon 50 (2012) 1993-1998. https://doi.org/10.1016/j.carbon.2011.12.057.

[33] R. Shu, X. Jiang, J. Li, Z. Shao, D. Zhu, T. Song, Z. Luo, Microstructures and mechanical properties of Al-Si alloy nanocomposites hybrid reinforced with nano-carbon and in-situ Al2O3, J. Alloy. Compd. 800 (2019) 150-162. https://doi.org/10.1016/j.jallcom.2019.06.030.

[34] D. Shin, A. Shyam, S. Lee, Y. Yamamoto, J.A. Haynes, Solute segregation at the Al/θ′-Al2Cu interface in Al-Cu alloys, Acta Mater. 141 (2017) 327-340. https://doi.org/10.1016/j.actamat.2017.09.020.

[35] Y. Ma, H. Chen, M. Zhang, A. Addad, Y. Kong, M. Lezaack, W. Gan, Z. Chen, G. Ji, Break through the strength-ductility trade-off dilemma in aluminum matrix composites via precipitation-assisted interface tailoring, Acta Mater. 242 (2023) 118470. https://doi.org/10.1016/j.actamat.2022.118470.

[36] F. Wang, J. Zhang, K. Sun, L. Quan, J. Wang, N. Zhao, C. Shi, S. Zheng, Synergistic reinforcement effect of Fe and in-situ synthesized MgAlB4 whiskers in Al matrix composites, Compos. Pt. B-Eng. 246 (2022) 110267. https://doi.org/10.1016/j.compositesb.2022.110267.

[37] Z. Li, G. Fan, Q. Guo, Z. Li, Y. Su, D. Zhang, Synergistic strengthening effect of graphene-carbon nanotube hybrid structure in aluminum matrix composites, Carbon 95 (2015) 419-427. https://doi.org/10.1016/j.carbon.2015.08.014.

[38] A. Nieto, D. Lahiri, A. Agarwal, Nanodynamic mechanical behavior of graphene nanoplatelet-reinforced tantalum carbide, Scr. Mater. 69 (2013) 678-681. https://doi.org/10.1016/j.scriptamat.2013.07.030.

[39] J. Liu, C. Liu, H. Cai, C. Zhang, C. Dan, Q. Shi, H. Wang, Z. Chen, Enhanced precipitate strengthening in particulates reinforced Al-Zn-Mg-Cu composites via bimodal structure design and

optimum aging strategy, Compos. Pt. B-Eng. 260 (2023) 110772. https://doi.org/10.1016/j.compositesb.2023.110772.

[40] J. Wang, Q. Zhou, S. Shao, A. Misra, Strength and plasticity of nanolaminated materials, Mater. Res. Lett. 5 (2017) 1-19. https://doi.org/10.1080/21663831.2016.1225321.

[41] Y. Jiang, Z. Tan, G. Fan, L. Wang, D. Xiong, Q. Guo, Y. Su, Z. Li, D. Zhang, Reaction-free interface promoting strength-ductility balance in graphene nanosheet/Al composites, Carbon 158 (2020) 449-455. https://doi.org/10.1016/j.carbon.2019.11.010.

[42] X. Kai, Z. Li, G. Fan, Q. Guo, D. Xiong, W. Zhang, Y. Su, W. Lu, W. Moon, D. Zhang, Enhanced strength and ductility in particulate-reinforced aluminum matrix composites fabricated by flake powder metallurgy, Mater. Sci. Eng. A-Struct. Mater. Prop. Microstruct. Process. 587 (2013) 46-53. https://doi.org/10.1016/j.msea.2013.08.042.

[43] S. Madeira, G. Miranda, V.H. Carneiro, D. Soares, F.S. Silva, O. Carvalho, The effect of SiCp size on high temperature damping capacity and dynamic Young's modulus of hot-pressed AlSi-SiCp MMCs, Mater. Des. 93 (2016) 409-417. https://doi.org/10.1016/j.matdes.2015.12.147.

[44] H. Zhang, D. Yang, X. Chen, H. Nagaumi, Z. Wu, C. Guo, J. Zou, P. Wang, K. Qin, J. Cui, Influence of Ag on microstructure, mechanical properties and tribological properties of as-cast Al-33Zn-2Cu high-zinc aluminum alloy, J. Alloy. Compd. 922 (2022) 166157. https://doi.org/10.1016/j.jallcom.2022.166157.

[45] N. Kalantarrashidi, M. Alizadeh, S. Pashangeh, Microstructure evolution and mechanical properties evolution of high-Zn Al-Zn alloys prepared by cross accumulative roll bonding combined with heat treatment process, J. Alloy. Compd. 927 (2022) 167042. https://doi.org/10.1016/j.jallcom.2022.167042.

[46] D.S. Prasad, C. Shoba, Damping Behavior of Metal Matrix Composites, Trans. Indian Inst. Met. 68

(2015) 161-167. https://doi.org/10.1007/s12666-014-0462-z.

[47] Z. Ma, F. Han, J. Wei, J. Gao, Effects of macroscopic defects on the damping behavior of aluminum and Zn-27 Pct Al alloy, Metall. Mater. Trans. A-Phys. Metall. Mater. Sci. 32 (2001) 2657-2661. https://doi.org/10.1007/s11661-001-0056-3.

[48] H. Jiang, C. Liu, Z. Ma, X. Zhang, L. Yu, M. Ma, R. Liu, Fabrication of Al–35Zn alloys with excellent damping capacity and mechanical properties, J. Alloy. Compd. 722 (2017) 138-144. https://doi.org/10.1016/j.jallcom.2017.06.091.

[49] J. Zhang, R.J. Perez, E.J. Lavernia, Documentation of damping capacity of metallic, ceramic and metal-matrix composite materials, J. Mater. Sci. 28 (1993) 2395-2404. https://doi.org/10.1007/bf01151671.

[50] J. Zhang, R.J. Perez, E.J. Lavernia, Dislocation-induced damping in metal matrix composites, J. Mater. Sci. 28 (1993) 835-846. https://doi.org/10.1007/bf01151266.

[51] C. Liu, H. Jiang, B. Zhang, Z. Ma, High damping capacity of Al alloys produced by friction stir processing, Mater. Charact. 136 (2018) 382-387. https://doi.org/10.1016/j.matchar.2018.01.009.

[52] X. Meng, D. Zhang, W. Zhang, C. Qiu, D. Chen, Achieving high damping capacity and strength simultaneously in a high-zinc aluminum alloy via melt spinning and hot extrusion, Mater. Sci. Eng. A-Struct. Mater. Prop. Microstruct. Process. 833 (2022) 142376. https://doi.org/10.1016/j.msea.2021.142376.

[53] X. Sun, F. Jiang, D. Yuan, G. Wang, Y. Tong, J. Wang, High damping capacity of AlSi10Mg-NiTi lattice structure interpenetrating phase composites prepared by additive manufacturing and pressureless infiltration, J. Alloy. Compd. 905 (2022) 164075. https://doi.org/10.1016/j.jallcom.2022.164075.

[54] D. Siva Prasad, C. Shoba, Experimental evaluation onto the damping behavior of Al/SiC/RHA

hybrid composites, J. Mater. Res. Technol-JMRT 5 (2016) 123-130. https://doi.org/10.1016/j.jmrt.2015.08.001.

[55] Z. Li, Q. Guo, Z. Li, G. Fan, D. Xiong, Y. Su, J. Zhang, D. Zhang, Enhanced mechanical properties of graphene (reduced graphene oxide)/aluminum composites with a bioinspired nanolaminated structure, Nano Lett. 15 (2015) 8077-8083. https://doi.org/10.1021/acs.nanolett.5b03492.

[56] M. Zhao, D. Xiong, Z. Tan, G. Fan, Q. Guo, C. Guo, Z. Li, D. Zhang, Lateral size effect of graphene on mechanical properties of aluminum matrix nanolaminated composites, Scr. Mater. 139 (2017) 44-48. https://doi.org/10.1016/j.scriptamat.2017.06.018.

[57] X. Meng, D. Zhang, W. Zhang, C. Qiu, G. Liang, J. Chen, Microstructure and mechanical properties of a high-Zn aluminum alloy prepared by melt spinning and extrusion, J. Alloy. Compd. 819 (2020) 152990. https://doi.org/10.1016/j.jallcom.2019.152990.

[58] Y. Lin, S. Mao, Z. Yan, Y. Zhang, L. Wang, The enhanced microhardness in a rapidly solidified Al alloy, Mater. Sci. Eng. A-Struct. Mater. Prop. Microstruct. Process. 692 (2017) 182-191. https://doi.org/10.1016/j.msea.2017.03.052.